Plasma metabolic signatures for intracranial aneurysm and its rupture identified by pseudotargeted metabolomics

Kaijian Sun
Zhujiang Hospital, Southern Medical University
Xin Zhang
Zhujiang Hospital, Southern Medical University
Xin Li
Zhujiang Hospital, Southern Medical University
Xifeng Li
Zhujiang Hospital, Southern Medical University
Shixing Su
Zhujiang Hospital, Southern Medical University
Yunhao Luo
Zhujiang Hospital, Southern Medical University
Hao Tian
Zhujiang Hospital, Southern Medical University
Meiqin Zeng
Zhujiang Hospital, Southern Medical University
Cheng Wang
Zhujiang Hospital, Southern Medical University
Yugu Xie
Zhujiang Hospital, Southern Medical University
Nan Zhang
Zhujiang Hospital, Southern Medical University
Ying Cao
Zhujiang Hospital, Southern Medical University
Zhaohua Zhu
The National Key Clinical Specialty, Southern Medical University
Qianlin Ni
Wuhan Metware Biotechnology Co., Ltd
Wenchao Liu
Zhujiang Hospital, Southern Medical University
Fangbo Xia

Zhujiang Hospital, Southern Medical University

Xuying He

Zhujiang Hospital, Southern Medical University

Zunji Shi

Lanzhou University

Chuanzhi Duan

Zhujiang Hospital, Southern Medical University

Haitao Sun (✉ 2009sht@smu.edu.cn)

Zhujiang Hospital, Southern Medical University

Research Article

Keywords: intracranial aneurysm, biomarkers, mass spectrometry, metabolomics, machine learning.

Posted Date: May 31st, 2022

DOI: https://doi.org/10.21203/rs.3.rs-1667277/v1

Abstract

Background

Whole-body metabolism is emerging as a critical player in the pathophysiology of intracranial aneurysms (IAs). However, the vital metabolic signatures for IA risk stratification and its potential biological underpinnings remain elusive. Therefore, our study aimed to develop an early diagnosis model and rupture classification model by analyzing plasma metabolic profiles of IA patients.

Methods

Plasma samples from a cohort of 105 participants, including 75 patients with IAs in ruptured and unruptured statuses and 30 control participants, were collected for analysis. A pseudotargeted metabolomics strategy based on LC-MS/MS was applied for integration analyses of plasma samples, and significant differential metabolites were identified through univariate and multivariate statistical analysis. Furthermore, an integrated machine learning strategy based on LASSO, random forest and logistic regression were used for feature selection and model construction.

Results

The composition of metabolites changed significantly with the severity of IA. Among them, glutathione metabolism and bile acid metabolism may play a crucial role. Two sets of biomarker panels (M6 & M5) were defined to discriminate IA and its rupture with the area under receiver operating characteristic curve (AUC) of 0.843 and 0.929 on the validation sets, respectively.

Conclusion

The present study comprehensively characterizes plasma metabolites in different statuses of IA and demonstrates the potential of metabolic markers as non-invasive risk diagnostic tools for IA.

Introduction

Intracranial aneurysms (IAs) are abnormal bulges that develop from the wall of intracranial arteries, affecting about 3–5% of adult populations [1]. Although IAs is a prevalent cerebrovascular disease worldwide, there are currently no approved biomarkers to readily assess disease progression. Moreover, the insidious course of IAs may lead to a propensity to misdiagnose at the early stage. The mortality rate of the first rupture of an aneurysm is 30%-40%. As for re-rupture aneurysmal cases, the mortality rate may reach up to 60%-70%, laying burdens on patients, families and society [2]. Current diagnosis of intracranial aneurysms requires heavy reliance on imaging techniques and the clinical assessment of high-risk aneurysms depends greatly on the clinician's experience, mainly according to the clinical factors,

hemodynamics and morphology of IA [3]. In addition, there is still a lack of validated biomarkers for early diagnosis and risk assessment of IA, which causes difficulties for large-scale screening. Moreover, once an unruptured intracranial aneurysm is detected, decisions regarding optimum management are still controversial [3, 4]. In this regard, it is of immense value to develop biological signatures that assist in the early diagnosis of IA and the prediction or classification of IA rupture.

In recent years, plasma metabolites as potential biomarkers have received enormous attention and have been an emerging field of research on IA. Previous studies have found several metabolic abnormalities of amino acids and fatty acids in patients with unruptured intracranial aneurysm (UIA) [5], suggesting that plasma metabolites were closely related to UIA. However, targeted studies of amino acids and fatty acids focused only on fewer metabolites and cannot globally reflect the overall metabolism of different IAs statuses. Additionally, widely targeted metabolomics [6, 7] are rarely used to discover biomarkers for early diagnosis of IA and rupture risk assessment. Pseudotargeted metabolomics can monitor hundreds to thousands of metabolites by dynamic multiple reaction monitoring, which merges the advantages of untargeted and targeted metabolomics with high sensitivity, high specificity and excellent quantification ability [8, 9]. Therefore, we hypothesized that significant differences in plasma metabolites could be identified in control subjects, UIA and RIA patients using this novel approach.

The present study aimed to describe the profiling of plasma metabolic characteristics and compare the difference among various statuses of IA patients using a widely targeted metabolomics method [7, 10]. Moreover, to explore the novel biomarkers for IAs, the classifiers based on the machine learning algorithm of least absolute shrinkage and selection operator (LASSO) and random forest were used to establish the IAs diagnosis model and rupture discrimination model. In addition, this study also aimed to explore potential biological functions and metabolic pathways of different metabolites so as to provide clues to novel diagnostic, preventive and therapeutic strategies against IA and its rupture. Based on the differential metabolite analysis of plasma samples from 105 participants, including 30 control participants and 75 patients with IA, we found that the composition of metabolic profile changed significantly with the severity of IAs. The two models we established with integrated machine learning strategies could effectively distinguish the aneurysm status. The results of receiver operating characteristic curve (ROC) showed strong predictive power. Our findings highlighted the role of specific metabolites as novel early diagnosis and risk assessment tools for IA.

Materials And Methods

Study design and participants

The study was conducted according to the guidelines laid down in the Declaration of Helsinki, and approval for the study was obtained from the Ethics Committee of Zhujiang Hospital, Southern Medical University (reference number: 2021-KY-038-02). Informed consent has been obtained for utilizing samples for research, with prior approval by the clinical Biobank Centre at Zhujiang Hospital of Southern Medical

University (approval number 2020-YBK-001-02). The study adheres to STROBE statement reporting guidelines.

Patients with IA in different statuses (asymptomatic UIA patients and RIA patients immediately after onset) and control participants (age and gender-matched) without aneurysmal symptoms or a history of subarachnoid hemorrhage were prospectively recruited for analysis in this study at Zhujiang Hospital of Southern Medical University from June 2020 to June 2021. For the disease groups, patients were diagnosed and grouped based on digital subtraction angiography (DSA) imaging and clinical records. IAs patients were further divided into two groups as follows: (1) untreated patients with unruptured intracranial aneurysms, (2) patients with ruptured intracranial aneurysms (RIAs) immediately after onset. Exclusion criteria were as follows: (1) aged <18 years, (2) having non-aneurysmal subarachnoid hemorrhage or treated UIAs before sample collection, (3) complicated with serious diseases such as cancer, persistent infectious disease or , (4) no diagnostic DSA images of IAs or incomplete clinical data.

Sample collection and storage

For disease groups, blood samples were collected prior to the endovascular coiling or microsurgical clipping before giving any anesthetic agent or any treatment. For the control group, blood samples were collected from participants who participated in the physical examination. Blood samples were collected in EDTA tubes by qualified medical personnel and centrifuged at 3000 rpm for 10 min at 4 ℃ to obtain aliquots of plasma and stored at -80℃ for subsequent metabolites detection.

Metabolomic study

Sample preparation and extraction. The plasma sample was thawed on ice, vortexed for 10 s and mixed well, 300 μL of pure methanol was added to 50 μL of plasma, and then the mixture was whirled for 3 min and centrifuged for 10 min at 12,000 rpm at 4 °C. Then, the supernatant was collected after centrifugation (12,000 rpm at 4°C for 5 min). Leave the supernatant in a refrigerator at -20°C for 30 min, centrifuge it at 12000 rpm at 4°C for 3 min, and take 150 μL of supernatant in the liner of the corresponding injection bottle for on-board analysis.

T3 UPLC Conditions. The sample extracts were analyzed using an LC-ESI-MS/MS system (UPLC, ExionLC AD, https ://sciex. com.cn/, MS, QTRAP® System, https://sciex.com/) [11]. The analytical conditions were as follows: UPLC column, Waters ACQUITY UPLC HSS T3 C18 (1.8μm, 2.1 mm*100 mm), column temperature, 40 °C, flow rate, 0.4 mL/min, injection volume, 2 μL or 5 μL, solvent system, water (0.1% formic acid): acetonitrile (0.1% formic acid), gradient program, 95:5 V/V at 0 min, 10:90 V/V at 10.0 min, 10:90 V/V at 11.0 min, 95:5 V/V at 11.1 min, 95:5 V/V at 14.0 min.

QTOF-MS/MS. The Triple TOF mass spectrometer was used for its ability to acquire MS/MS spectra on an information dependent basis (IDA) during an LC/MS experiment [12]. In this mode, the acquisition software (Triple TOF 6600, AB SCIEX) continuously evaluates the full scan survey MS data as it collects and triggers the acquisition of MS/MS spectra depending on preselected criteria. In each cycle, 12

precursor ions whose intensity greater than 100 were chosen for fragmentation at collision energy (CE) of 30 V (12 MS/MS events with product ion accumulation time of 50 msec each). ESI source conditions were set as following: Ion source gas 1 as 50 Psi, Ion source gas 2 as 50 Psi, Curtain gas as 25 Psi, source temperature 500 °C, Ion Spray Voltage Floating (ISVF) 5500 V or -4500 V in positive or negative modes, respectively.

ESI-Q TRAP-MS/MS. LIT and triple quadrupole (QQQ) scans were acquired on a triple quadrupole-linear ion trap mass spectrometer (QTRAP), QTRAP® LC-MS/MS System, equipped with an ESI Turbo Ion-Spray interface, operated in positive and negative ion mode and controlled by Analyst 1.6.3 software (Sciex). The ESI source operation parameters were as follows: source temperature 500 °C, ion spray voltage (IS) 5500 V (positive), -4500 V (negative), ion source gas I (GSI), gas II (GSII), curtain gas (CUR) were set at 50, 50, and 25.0 psi, respectively, the collision gas (CAD) was high. Instrument tuning and mass calibration were performed with 10 and 100 μmol/L polypropylene glycol solutions in QQQ and LIT modes, respectively. A specific set of MRM transitions were monitored for each period according to the metabolites eluted within this period [13].

Quality control (QC) samples were a mixture of all sample extracts, which were inserted into the queue to monitor the stability of the detection method. PCA plot was used to estimate the degree of variability and the overall metabolic difference.

Data processing and statistical analysis

The raw data were represented by the area under the ion intensive peaks. In total, we confirmed 501 metabolites after removing unknown substances and interferon ion pairs for further analysis. The data normalized with log2 transformation and standard with z-score. We conducted unsupervised analysis PCA (principal component analysis) and supervised analysis Orthogonal Projections to Latent Structures Discriminant Analysis （OPLS-DA）to evaluate the profiling of metabolites in each group, and performed permutation in 200 times to validate the power of our modeling, all of which were using R package *"prcomp", "MetaboAnalystR"* （R version 3.6.1）, and SIMCA software [14].

The univariance analysis with normally distributed variables between two groups was analyzed by Student's t-test, while non-normally distributed were analyzed by Mann-Whitney test. Categorical variables were compared by the χ 2 test or Fisher's exact test using SPSS26.0. Selected significant difference metabolites between every two groups （UIA *vs.* Control, RIA *vs*. UIA）were determined by Variable influence on projection (VIP) ≥1, *p*-value <0.05 (FDR<0.1), and fold change (FC, based on mean) ≥1.2 or FC ≤0.83. We also conducted pathway enrichment analysis based on the KEGG Pathway database (http://www.kegg.jp/kegg/pathway.html) [15].

Machine-learning strategy

The multivariance analysis was used in two machine learning methods, including least absolute shrinkage and selection operator (LASSO) and random forest (RF) [16], to further select candidate

biomarkers from significantly different metabolites by using R package "*glmnet"* and R package "*varSelRF"* separately (R version 3.6.1) [17]. Briefly, for each comparison, the data subset was randomly divided into a training set and a verification set in 2:1. Then, 500 times selection of LASSO and 10-fold cross-validation (CV) to determine the candidate metabolites with optimal parameter lambda and select markers by random forest (RF). Finally, the candidate biomarkers were figured out both in LASSO and RF and were ranked using the LASSO non-zero coefficients and RF mean decrease of accuracy. The logistic regression model fitted by several combinations of biomarkers, and receiver operating characteristic curve (ROC) with the calculation of AUC were completed by R package "*pROC"* [18].

Results

Clinical and demographic characteristics of the study cohorts

A concise workflow of the entire study design is shown in figure 1. Totally, 105 plasma samples including 75 from patients with IAs in different statuses and 30 from control participants were collected for analysis in this study. Characteristics of the UIAs, RIAs patients and control participants are shown in Table 1. As shown, there were no significant differences between groups in terms of demographic factors (age, sex and tobacco use). However, the control participant had a lower prevalence of hypertension than the disease groups but there were no differences between UIA and RIA. Additionally, there were no differences among the three groups in regard to the prevalence of other comorbidities such as cardiac disease (myocardial infarction and angina), hyperlipemia, stroke history and diabetes mellitus. In terms of aneurysm characteristics, UIA often occurred in the internal carotid artery while irregular morphology was observed more commonly in RIA. (Table 1).

Plasma metabolic profiling of all samples

A total of 501 metabolites were detected using hydrophilic and hydrophobic methods by UHPLC-TQMS. Our results showed that the QC samples were clustered together, indicating the stability of this analytic method (Supplement figure 1A). In addition, the method stability was assessed by overlaying different samples' total ion current diagrams (TIC diagrams). The results showed that the curves of the TIC diagrams were highly overlapped, and the retention time and peak intensity were consistent, demonstrating that the signals were stable throughout the analysis process (Supplement figure 1B).

Comparison of plasma metabolic profiling between the UIA and control groups

Firstly, to identify the metabolites associated with aneurysm formation, we focused on the differential metabolites between UIA and controls. Using the OPLS-DA model, the classification results showed a significant separation of all plasma metabolites between UIAs and controls (Figure 2A). The top20 VIP metabolites included various adenosine metabolites (Supplement Figure 3A). Next, we performed a univariate T-test analysis based on the fold changes of metabolites in the two groups and found 19 metabolites with *p*-value <0.05 (FDR<0.1) and VIP>1, in which 11 metabolites decreased and eight metabolites increased in UIAs, as shown in the volcano plot (Figure 2B). By comparison, the top

foldchange metabolites result showed that the abundance of amino acid and its metabolomics was upregulated. Meanwhile, some derivatives of benzene and nucleotide were generally declined in UIAs (Figure 2C).

Besides, clustering analysis of these 19 significantly altered metabolites showed a clear separation in the heatmap (Supplement Figure 2A). KEGG pathway enrichment analysis of differential metabolites showed that phosphonate and phosphinate metabolism had the highest risk factor. There are mainly nine significantly disturbed metabolic pathways such as glutathione metabolism, biosynthesis of amino acids and cofactors (Figure 2D).

Comparison of plasma metabolic profiling between the RIA and UIA groups

Furthermore, special attention was given to the transition from a stable aneurysm to rupture and subarachnoid haemorrhage. OPLS-DA models of metabolic profiling data indicated that the overall plasma metabolites were significantly different among the various statuses of IAs patients (Figure 3A), suggesting that these two disease stages had distinct metabolic profiles at the molecular level. The top20 VIP metabolites included indole and arachidonic acid (Supplement Figure 3B).By univariate analysis, 172 differential metabolites between RIAs and UIAs were identified, of which 69 were upregulated and 103 were downregulated (Figure 3B). All of these significantly altered metabolites clustered well in the heatmap (Supplement Figure 2B). The top downregulated foldchange metabolites mainly include various secondary bile acids, for example glycochenodeoxycholic acid, glycine deoxycholic acid and so on (Figure 3C). These differential metabolites were enriched in 6 pathways with the highest risk factor, including linoleic acid metabolism, vascular smooth muscle contraction, fatty acid metabolism, phosphonate and phosphinate metabolism, retrograde endocannabinoid signaling and serotonergic synapse (Figure 3D).

Machine-learning-based selection of biomarker panels for classification of RIA and UIA

After systematically defining the metabolomic profiles and pathways associated with UIAs and RIAs, we set out to establish a diagnostic model by selecting metabolites that could be used to predict the presence of UIA and differentiate RIA from UIA. The metabolites obtained after preliminary statistical screening are still numerous ($p<0.05$, $FC>1.2$). To further narrow down the biomarker candidates, we applied a variable selection method to screen for important metabolites. Variable selection is to select a set of independent variables that have strong explanatory power for the dependent variable from a large number of independent variables through statistical analysis methods, and is an essential part of statistical inference. Here, all samples were randomly split into training and validation sets in a 2:1 ratio. LASSO and Random Forest were used to select metabolites, and then their intersections are candidate metabolites, served as the optimal biomarkers. To improve predictive performance and avoid overfitting and false positives, we performed 500 times feature selection and 10-fold cross validation on the training set [19]. Logistic regression was used for final model building based on optimal biomarkers, which were evaluated by AUC value of ROC curve and prediction accuracy in the validation set (Figure 4A).

By utilizing the above machine-learning strategy, we identified a diagnostic panel to predict the presence of UIA (UIA versus control) containing six metabolites (dubbed M6), including N-Acetyl-L-Leucine, porphobilinogen, ethylsalicylate, ethionamide, N6-methyladenosine and 1-Methyladenosine. The diagnostic model distinguished UIA from control with an AUC of 0.9 in training set (Figure 4B), 0.843 in validation set (Figure 4C) and 0.882 in all samples (Supplement Figure 4A) with high sensitivity and specificity. The prediction effect of the model was rendered by scatter plots to evaluate the reliability of the machine-learning strategy, and the results demonstrated that different samples could be correctly classified with a high accuracy of 19/24 on the validation set (Figure 4D).

We further explored the possibility of distinguishing different statuses of IA patients (RIA versus UIA). The optimal biomarkers or rupture prediction model that had similar performance in two machine learning methods consisted of five metabolites (dubbed M5), including glycochenodeoxycholic acid, 5,6-dimethylbenzimidazole, uracil, catechol and N-(1-Deoxy-1-fructosyl) phenylalanine. The rupture prediction model distinguishing RIAs from UIAs yielded an AUC of 0.99 in the training set (Figure 4E), 0.929 in the validation set (Figure 4F) and 0.933 in all samples (Supplement Figure 4B). The scatter plot shows good prediction effect of the model for the RIA group and UIA group with accuracy of 23/25 (Figure 4G).

Finally, the abundances of M6 in diagnostic model showed statistical significance both on the training set and validation set implying their potential as biomarkers to distinguish UIA (Figure 5A). While most biomarkers in rupture prediction model also showed consistent significant difference, but glycochenodeoxycholic acid and 5,6-dimethylbenzimidazole only showed a downward trend in the validation set of RIA (Figure 5B).

Discussion

Herein we performed a pseudotargeted metabolomics study to systematically define the metabolic profiles and related pathways in the development of IA. The metabolomic profile analysis showed significantly diverse pathways in UIAs patients compared to control participants, among which glutathione metabolism emerges as the most significantly altered. Furthermore, two pathways appear to play a crucial role in the progression from UIA to RIA. Moreover, we developed a comprehensive biomarker discovery strategy to further select and structurally validate two panels of six- and five-metabolites based biomarker combinations with potential clinical utility for classifying UIA and its rupture using two machine learning algorithms (LASSO and random forest), which are increasingly recognized as an effective method to evaluate and predict disease states [20]. The plasma biomarker panel distinguished UIAs from the controls with dramatically high performance with AUC of 0.9 in the training set and 0.843 in the validation set. More importantly, we developed a prediction model based on five metabolites to distinguish RIA patients from UIA, with high effectiveness: AUCs in the training and validation sets ranged from 0.99 to 0.929, respectively. Our findings highlighted the role of specific metabolites as novel early diagnosis and risk biomarkers for IA. The metabolites we selected achieved excellent diagnostic and predictive power. The ROC curve indicated the potential biomarker panels would be suitable for diagnosis and rupture risk assessment of IAs.

Intracranial aneurysms result in high morbidity and mortality due to a significant rate of asymptomatic carrying rate and cause damage to the nervous system after rupture [21]. Although DSA is currently the gold standard for the diagnosis and risk assessment of IAs [22], regular and repeated invasive examinations are challenging to perform in large scale population screening because of health risk, subjective variation in imaging interpretation, and cost [23]. Thus, in this regard, an urgent need is required to establish and validate biomarkers with high specificity and accuracy for early diagnosis, dynamic monitoring and assessment of IA rupture risk. With rapid technological evolution, metabolomics is increasingly being used to define predictive biomarkers for diseases, particularly cardiovascular disease, and is increasingly becoming a blueprint for understanding the pathophysiological mechanisms of disease. Our study provided a comprehensive picture of metabolites in the entire spectra of IA patients and determined potential biomarkers for its detection and risk assessment, allowing a better understanding of the pathologic process of IA.

There are several notable findings. The metabolic profile analysis showed significantly altered pathways in patients with UIA compared to controls, among which glutathione metabolism emerges as the most significantly dysregulated. Recent research indicated that upregulation of glutathione metabolism could increase the production of reactive oxygen species (ROS), which plays a vital role in the pathogenesis of IAs [24]. And it also enhances vascular endothelial growth factor receptor 2 (VEGFR2) activation, which is a fundamental regulator of angiogenesis and plays an important role in vascular smooth muscle cell phenotypic modulation [25]. Correspondingly, our study showed that glycine and L-ornithine increased significantly in UIA patients in this pathway. Therefore, we hypothesize that these amino acid metabolites may contribute to IA formation through oxidative stress. Previous study has found significant metabolic abnormalities of amino acids and fatty acids in patients with unruptured aneurysms [5]. Our finding was consistent with it, but our results further suggested that fatty acid metabolism mainly contributed to the progressive stage of IA. With the aggravation of IA, linoleic acid metabolism pathway and vascular smooth muscle contraction pathway were typically enriched. Specifically, arachidonic acid plays a vital role in both two pathways. Recent studies have found that arachidonic acid metabolites promote the occurrence, development and plaque instability of atherosclerosis [26], which is a risk factor for IA [27]. Therefore, it is reasonable to speculate that arachidonic acid plays a role in the progression of IA. Moreover, it is well known for the role of phenotypic transformation of vascular smooth muscle cells in the progression of IA [28, 29]. In our study, there existed characteristic enrichment of vascular smooth muscle contraction pathway accompanied by the decrease in adenosine content. At the same time, methylation-modified adenosine such as N6-methyladenosine and 1-methyladenosine, as biomarkers for the diagnostic model, are also significantly down-regulated in UIA. Therefore, we assume that these metabolites may be involved in decreasing vascular smooth muscle contractility.

Among the top fold changed metabolites between RIA and UIA, we were surprised to find a significant decrease in various glycine-conjugated secondary bile acids, of which glycochenodeoxycholic acid was also a biomarker in rupture prediction models. Glycochenodeoxycholic acid is produced by the action of enzymes existing in the microbial flora of the colonic environment [30]. Previous animal and human studies have demonstrated that alterations in gut microbiota contribute to the rupture of intracranial

aneurysms [31, 32]. Our study suggests that secondary bile acids may mediate the pathogenic effect of gut microbiota disturbance on IAs, which needs to be further confirmed in future studies. Subsequently, uridine and uracil decreased dynamically with the IA and its rupture. Uridine played a crucial role in the central nervous system and uridine administration had anti-epileptic actions [33]. Accordingly, drug target enrichment in a large-scale GWAS research showed pleiotropic characteristics of anti-epileptic drugs with the genetic association of intracranial aneurysms [34]. Therefore, our study raised the possibility that uridine may also have a potential treatment effect on IAs.

Despite the valuable results of our study, our research also has several limitations. Firstly, it was performed in small cohorts and was not fully validated in the prospective cohort study. Therefore, large, multicenter clinical trials will be needed to evaluate the precision and robustness of the two panels as non-invasive biomarkers for IAs. Secondly, taking into account the fact that the aneurysm rupture event itself can also cause the body's stress response, some metabolites that change significantly in the rupture group can only indicate the post-rupture state rather than a risk predictor. However, the metabolites involved in the pathologic process of intracranial aneurysms still have fundamental application prospects for rupture risk prediction, and it is worthwhile further to verify their mechanism through basic experiments in the future. Thirdly, other risk factors that may affect IAs were not involved in our study including genes and hemodynamic parameters. Moreover, the detailed roles of the biomarker metabolites in the pathogenesis of IA require further investigation on potential therapeutic targets, which must be further elucidated or experimentally validated.

Conclusions

In summary, our study has exemplified the power of combining metabolomics and machine learning algorithms for identifying potential metabolic biomarkers to discriminate UIA from controls and even predict the development of UIA. These prediction models demonstrate the potential of metabolic markers as non-invasive risk diagnostic tools for IA and may also be applied in epidemiologic settings to predict the percentage of individuals with UIAs at high risk of rupture. Such a novel approach may have a profound impact on the clinical assessment and management of IAs.

Declarations

Ethical Approval and Consent to participate

The study was conducted according to the guidelines laid down in the Declaration of Helsinki, and approval for the study was obtained from the Ethics Committee of Zhujiang Hospital, Southern Medical University (reference number: 2021-KY-038-02). Informed consent has been obtained for utilizing samples for research, with prior approval by the clinical Biobank Centre at Zhujiang Hospital of Southern Medical University (approval number 2020-YBK-001-02).

Consent for Publication

All authors have read and given consent for publication.

Data Availability

Additional data to that included in the manuscript can be provided under request.

Competing Interest

The authors declare that they have no competing interests.

Funding

This work was supported by the National Natural Science Foundation of China (81974178, 81974177), Guangdong Basic and Applied Basic Research Foundation (2020A1515010038) and the Presidential Foundation of Zhujiang Hospital of Southern Medical University (No. yzjj2018rc03).

Author contributions

HS and CD jointly conceptualized the study. HS and KS designed experiments and prepared the manuscript. ZS provided expertise and participated in the design of the experiments. XZ, XL, XL, SS, WC, YL, NZ, YX, DC, WL and XH collected the patient samples and information. ZS, KS, HS, QN, MZ, HT, CW, YC and FX analyzed the data. HS, ZS, CD and ZZ revised the manuscript. All authors read and approved the final manuscript.

Acknowledgements

We would like to thank Dr. Zhen Liu for technical assistance. We would also like to thank all staff at the Neurosurgery Centre and Cerebrovascular Surgery of Zhujiang Hospital of Southern Medical University, and the technical staff of the Clinical Biobank Centre for their kind assistance. We would also like to thank all staff at clinical Research Centre of Zhujiang Hospital for their support in overseeing the study. Finally, we thank all tissue donors and their families who have kindly donated their resected specimens to the Clinical Biobank Centre.

Author information

Kaijian Sun, Xin Zhang and Xin Li have contributed equally to this work and share first authorship.

Affiliations

Neurosurgery Center, Department of Cerebrovascular Surgery, Engineering Technology Research Center of Education Ministry of China on Diagnosis and Treatment of Cerebrovascular Disease, The National Key Clinical Specialty, Guangdong Provincial Key Laboratory on Brain Function Repair and Regeneration, The Neurosurgery Institute of Guangdong Province, Zhujiang Hospital, Southern Medical University, Guangzhou 510280, Guangdong, China.

Kaijian Sun, Xin Zhang, Xifeng Li, Shixing Su, Hao Tian, Meiqin Zeng, Cheng Wang, Nan Zhang, Ying Cao, Wenchao Liu, Xuying He, Chuanzhi Duan, Haitao Sun

Clinical Biobank Centre, Microbiome Medicine Center, Department of Laboratory Medicine, Zhujiang Hospital, Southern Medical University, Guangzhou 510280, Guangdong, China.

Xin Li2, Yunhao Luo, Yugu Xie, Fangbo Xia, Haitao Sun

Clinical Research Centre, Orthopedic Centre, Zhujiang Hospital, Southern Medical University, Guangzhou, 510280, China.

Zhaohua Zhu

Wuhan Metware Biotechnology Co., Ltd., Wuhan 430000, China.

Qianlin Ni

State Key Laboratory of Grassland Agro-ecosystems, Center for Grassland Microbiome, College of Pastoral Agriculture Science and Technology, Lanzhou University, Lanzhou, 730000, China.

Zunji Shi

Key Laboratory of Mental Health of the Ministry of Education, Guangdong–Hong Kong–Macao Greater Bay Area Centre for Brain Science and Brain-Inspired Intelligence, Southern Medical University, Guangzhou 510515, Guangdong, China.

Haitao Sun

Corresponding author

Correspondence to Zunji Shi, Chuanzhi Duan and Haitao Sun.

References

1. Etminan N, Rinkel GJ. Unruptured intracranial aneurysms: development, rupture and preventive management. Nat Rev Neurol. 2016;12:699–713.
2. Jaja BNR, Saposnik G, Lingsma HF, Macdonald E, Thorpe KE, Mamdani M, et al. Development and validation of outcome prediction models for aneurysmal subarachnoid haemorrhage: the SAHIT multinational cohort study.
3. Brown RD, Jr., Broderick JP. Unruptured intracranial aneurysms: epidemiology, natural history, management options, and familial screening.
4. Korja M, Kaprio J. Controversies in epidemiology of intracranial aneurysms and SAH.

5. Li H, Xu H, Li Y, Jiang Y, Hu Y, Liu T, et al. Alterations of gut microbiota contribute to the progression of unruptured intracranial aneurysms. Nat Commun. 2020;11:3218.
6. Muguruma Y, Tsutsui H, Noda T, Akatsu H, Inoue K. Widely targeted metabolomics of Alzheimer's disease postmortem cerebrospinal fluid based on 9-fluorenylmethyl chloroformate derivatized ultra-high performance liquid chromatography tandem mass spectrometry.
7. Zheng F, Zhao X, Zeng Z, Wang L, Lv W, Wang Q, et al. Development of a plasma pseudotargeted metabolomics method based on ultra-high-performance liquid chromatography-mass spectrometry. Nat Protoc. 2020;15:2519–37.
8. Li Y, Ruan Q Fau - Li Y, Li Y Fau - Ye G, Ye G Fau - Lu X, Lu X Fau - Lin X, Lin X Fau - Xu G, et al. A novel approach to transforming a non-targeted metabolic profiling method to a pseudo-targeted method using the retention time locking gas chromatography/mass spectrometry-selected ions monitoring.
9. Chen S, Kong H Fau - Lu X, Lu X Fau - Li Y, Li Y Fau - Yin P, Yin P Fau - Zeng Z, Zeng Z Fau - Xu G, et al. Pseudotargeted metabolomics method and its application in serum biomarker discovery for hepatocellular carcinoma based on ultra high-performance liquid chromatography/triple quadrupole mass spectrometry.
10. Chen W, Gong L Fau - Guo Z, Guo Z Fau - Wang W, Wang W Fau - Zhang H, Zhang H Fau - Liu X, Liu X Fau - Yu S, et al. A novel integrated method for large-scale detection, identification, and quantification of widely targeted metabolites: application in the study of rice metabolomics.
11. Chen Y, Zhang R, Song Y, He J, Sun J, Bai J, et al. RRLC-MS/MS-based metabonomics combined with in-depth analysis of metabolic correlation network: finding potential biomarkers for breast cancer. Analyst. 2009;134:2003–11.
12. Fraga CG, Clowers BH, Moore RJ, Zink EM. Signature-discovery approach for sample matching of a nerve-agent precursor using liquid chromatography-mass spectrometry, XCMS, and chemometrics. Anal Chem. 2010;82:4165–73.
13. Li M, Haixia Y, Kang M, An P, Wu X, Dang H, et al. The Arachidonic Acid Metabolism Mechanism Based on UPLC-MS/MS Metabolomics in Recurrent Spontaneous Abortion Rats. Front Endocrinol (Lausanne). 2021;12:652807.
14. Thevenot EA, Roux A, Xu Y, Ezan E, Junot C. Analysis of the Human Adult Urinary Metabolome Variations with Age, Body Mass Index, and Gender by Implementing a Comprehensive Workflow for Univariate and OPLS Statistical Analyses. J Proteome Res. 2015;14:3322–35.
15. Kanehisa M, Goto S. KEGG: kyoto encyclopedia of genes and genomes. Nucleic Acids Res. 2000;28:27–30.
16. Xie G, Wang X, Wei R, Wang J, Zhao A, Chen T, et al. Serum metabolite profiles are associated with the presence of advanced liver fibrosis in Chinese patients with chronic hepatitis B viral infection. BMC Med. 2020;18:144.
17. Xu RH, Wei W, Krawczyk M, Wang W, Luo H, Flagg K, et al. Circulating tumour DNA methylation markers for diagnosis and prognosis of hepatocellular carcinoma. Nat Mater. 2017;16:1155–61.

18. Robin X, Turck N, Hainard A, Tiberti N, Lisacek F, Sanchez JC, et al. pROC: an open-source package for R and S + to analyze and compare ROC curves. BMC Bioinformatics. 2011;12:77.
19. Yang QJ, Zhao JR, Hao J, Li B, Huo Y, Han YL, et al. Serum and urine metabolomics study reveals a distinct diagnostic model for cancer cachexia.
20. Xiong Y, Zheng Y, Yan Y, Yao J, Liu H, Shen F, et al. Circulating proteomic panels for risk stratification of intracranial aneurysm and its rupture. EMBO molecular medicine. 2022;14:e14713. https://doi.org/10.15252/emmm.202114713
21. Schatlo B, Fung C, Stienen MN, Fathi AR, Fandino J, Smoll NR, et al. Incidence and Outcome of Aneurysmal Subarachnoid Hemorrhage: The Swiss Study on Subarachnoid Hemorrhage (Swiss SOS).
22. van Rooij WJ, Sprengers Me Fau - de Gast AN, de Gast An Fau - Peluso JPP, Peluso Jp Fau - Sluzewski M, Sluzewski M. 3D rotational angiography: the new gold standard in the detection of additional intracranial aneurysms.
23. Zeng Y Fau - Liu X, Liu X Fau - Xiao N, Xiao N Fau - Li Y, Li Y Fau - Jiang Y, Jiang Y Fau - Feng J, Feng J Fau - Guo S, et al. Automatic Diagnosis Based on Spatial Information Fusion Feature for Intracranial Aneurysm.
24. Starke RM, Thompson JW, Ali MS, Pascale CL, Martinez LA, Ding D, et al. Cigarette Smoke Initiates Oxidative Stress-Induced Cellular Phenotypic Modulation Leading to Cerebral Aneurysm Pathogenesis. Arterioscler Thromb Vasc Biol. 2018;38:610–21.
25. Prasai PK, Shrestha B, Orr AW, Pattillo CB. Decreases in GSH:GSSG activate vascular endothelial growth factor receptor 2 (VEGFR2) in human aortic endothelial cells. Redox Biol. 2018;19:22–7.
26. Sonnweber T, Pizzini A, Nairz M, Weiss G, Tancevski I. Arachidonic Acid Metabolites in Cardiovascular and Metabolic Diseases. International journal of molecular sciences. 2018;19. https://doi.org/10.3390/ijms19113285
27. Shimonaga K, Matsushige T, Ishii D, Sakamoto S, Hosogai M, Kawasumi T, et al. Clinicopathological Insights From Vessel Wall Imaging of Unruptured Intracranial Aneurysms. Stroke. 2018;49:2516–9. https://doi.org/10.1161/strokeaha.118.021819
28. Starke RM, Chalouhi N, Ding D, Raper DM, McKisic MS, Owens GK, et al. Vascular smooth muscle cells in cerebral aneurysm pathogenesis. Transl Stroke Res. 2014;5:338–46. https://doi.org/10.1007/s12975-013-0290-1
29. Yan Y, Xiong J, Xu F, Wang C, Zeng Z, Tang H, et al. SDF-1α/CXCR4 Pathway Mediates Hemodynamics-Induced Formation of Intracranial Aneurysm by Modulating the Phenotypic Transformation of Vascular Smooth Muscle Cells. Transl Stroke Res. 2022;13:276–86. https://doi.org/10.1007/s12975-021-00925-1
30. Ma C, Han M, Heinrich B, Fu Q, Zhang Q, Sandhu M, et al. Gut microbiome-mediated bile acid metabolism regulates liver cancer via NKT cells. Science (New York, NY). 2018;360. https://doi.org/10.1126/science.aan5931

31. Shikata F, Shimada K, Sato H, Ikedo T, Kuwabara A, Furukawa H, et al. Potential Influences of Gut Microbiota on the Formation of Intracranial Aneurysm. Hypertension. 2019;73:491–6.
32. Kawabata S, Takagaki M, Nakamura H, Oki H, Motooka D, Nakamura S, et al. Dysbiosis of Gut Microbiome Is Associated With Rupture of Cerebral Aneurysms. Stroke. 2022;53:895–903. https://doi.org/10.1161/strokeaha.121.034792
33. Dobolyi A, Juhász G Fau - Kovács Z, Kovács Z Fau - Kardos J, Kardos J. Uridine function in the central nervous system.
34. Bakker MA-O, van der Spek RAA, van Rheenen WA-O, Morel SA-O, Bourcier R, Hostettler IA-O, et al. Genome-wide association study of intracranial aneurysms identifies 17 risk loci and genetic overlap with clinical risk factors.

Tables

Table 1 Demographic and clinical features of the study cohort

	Control(n=30)	UIAs(n=42)	RIAs(n=33)	P value
Patient characteristics				
Age, years*	51.00±12.67	53.31±10.65	58.36±11.51	0.066
Female§	17 (56.7%)	34 (81.0%)	23 (69.7%)	0.083
Tobacco use§	1 (3.3%)	2 (4.8%)	5 (15.2%)	0.14
Comorbidities§				
Hypertension	7 (23.3%)	21 (50%)	18 (54.5%)	0.026[a]
Cardiac disease	3 (10.0%)	1 (2.4%)	0	0.096
Hypercholesterolemia	2 (6.7%)	5 (11.9%)	1 (3.0%)	0.346
Stroke history	6 (20.0%)	4 (9.5%)	0	0.026
Diabetes mellitus	3 (10.0%)	3 (7.1%)	4 (12.1%)	0.762
Aneurysm characteristics§				
Multiplicity	NA	11 (26.2%)	14 (42.4%)	0.139
Regular morphology	NA	39 (92.9%)	15 (45.5%)	0.001[b]
Size#				
max diameter, mm	NA	4.30 (3.40,5.25)	5.00 (4.00,7.53)	0.288
Location§				0.006[b]
ICA	NA	29(69.0%)	8 (24.2%)	
MCA	NA	6 (14.3%)	7 (21.2%)	
PCA	NA	0	1 (3.0%)	
BA	NA	1 (2.4%)	2 (6.1%)	
AComA	NA	3(7.1%)	8 (24.2%)	
PComA	NA	3 (7.1%)	7 (21.2%)	

Table legend

* mean ± SD, § n (%), # median (IQR).

For the difference comparison of clinical characteristics among the three groups, one-way analysis of variance (ANOVA) was employed in cases of continuous normally distributed data. Non-normally distributed variables between two groups were analyzed by Mann-whitney test. Categorical variables were compared by the χ2 test.

Hypertension is defined as blood pressure≥140/90mmHg. Cardiac disease is defined as history of myocardial infarction or angina. NA: not available, ICA: internal carotid artery, MCA: middle cerebral artery, PCA: posterior cerebral artery, BA: basilar artery, AComA: anterior communicating artery, PComA: posterior communicating artery.

[a] $P < 0.05$ for equality among control, UIA and RIA. [b] $P < 0.05$ for equality between UIA and RIA.

Figures

Figure 1

Study design and workflow of biomarker discovery in intracranial aneurysms.

UIA= unruptured intracranial aneurysm, RIA= ruptured intracranial aneurysm, TOF= time-of-flight, MRM= multiple reaction monitoring, PCA = principal components analysis, OPLS- DA = orthogonal partial least squares discriminant analysis, LASSO= least absolute shrinkage and selection operator, ROC = receiver operating characteristic.

Figure 2

Metabolic profiles distinguishing unruptured intracranial aneurysm (UIA) patients from controls

(A) OPLS-DA score plots of UIA patients and control participants. (B) Volcano plots of UIA patients and control participants. $\log_2FC > \log_2 1.2$ or $< -\log_2 1.2$, $-\log_{10}FDR > 1$ were considered as significant. (C) Bar graphs presented as $\log_2FC$ of significantly different metabolites between UIA patients and control participants. (D) KEGG enrichment bubble plots of UIA patients and control participants. The color of bubbles represents the value of adjusted p value and the pathways of $p < 0.05$ are marked in the figure. The size of bubbles represents the number of counts (sorted by gene ratio).

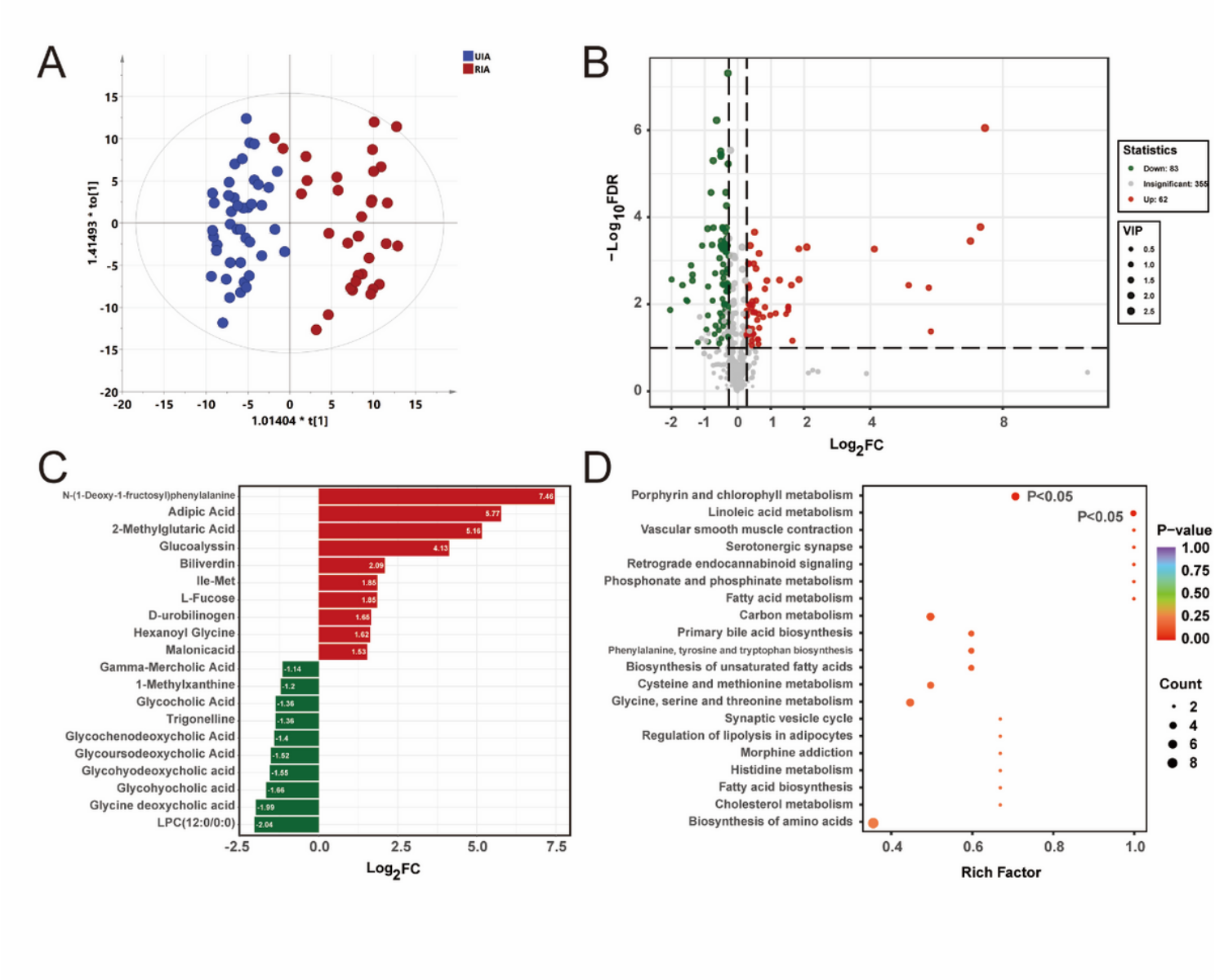

Figure 3

Metabolic profiles distinguishing ruptured intracranial aneurysm (RIA) patients from UIA patients

(A) OPLS-DA score plots of RIA patients and UIA patients. (B) Volcano plots of RIA patients and UIA patients. $\log_2$FC > $\log_2$1.2 or < -$\log_2$1.2, -$\log_{10}$FDR> 1 were considered as significant. (C) Bar graphs presented as $\log_2$FC of significantly different metabolites between RIA patients and UIA patients. (D) KEGG enrichment bubble plots of RIA patients and UIA patients. The color of bubbles represents the value of adjusted p value and the pathways of p< 0.05 are marked in the figure. The size of bubbles represents the number of counts (sorted by gene ratio).

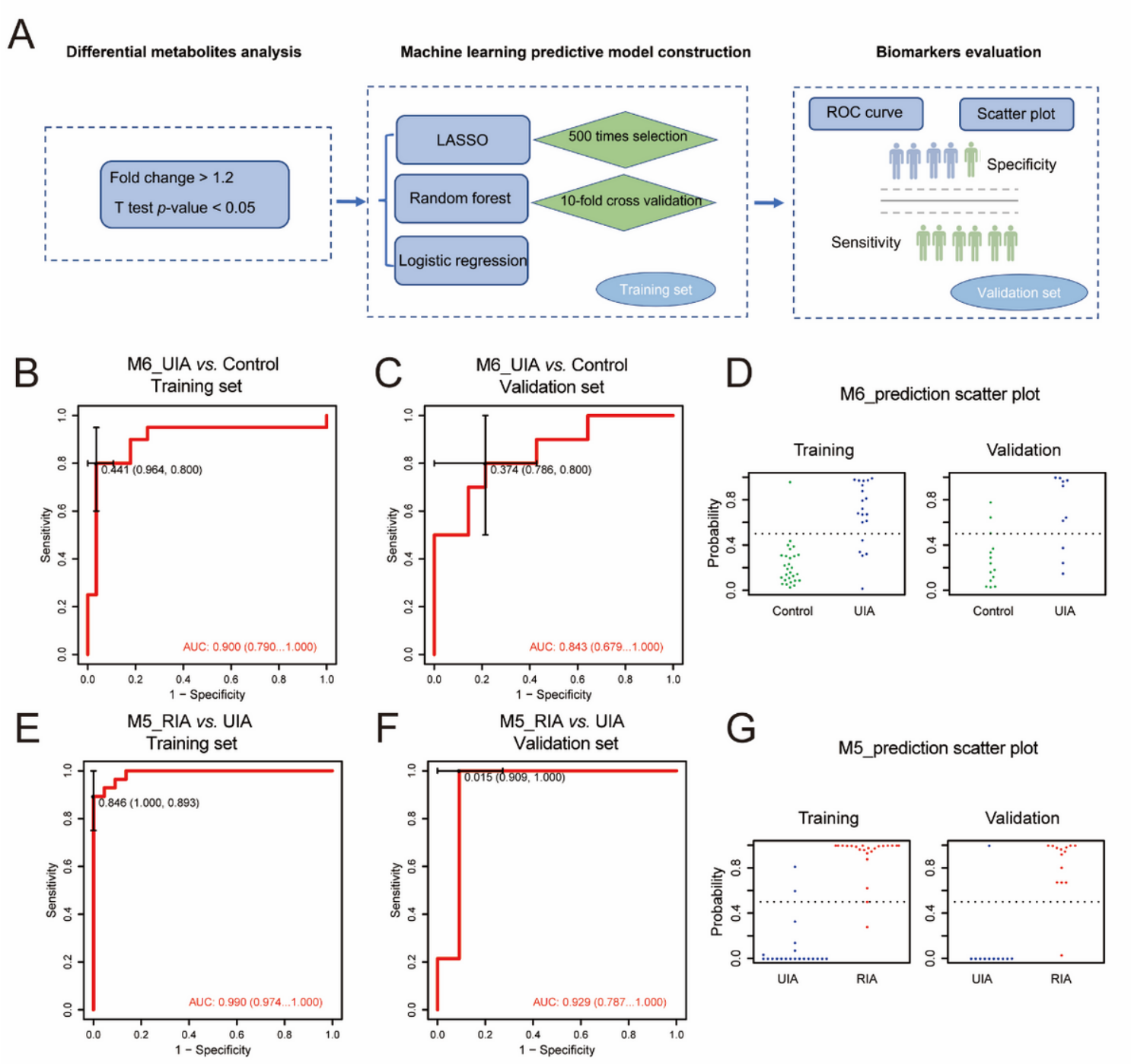

Figure 4

Potential biomarker panels for predicting the presence of UIA and differentiate RIA from UIA

(A) Workflow for biomarker discovery identified by integrated machine learning method. (B) ROC curve of potential plasma metabolites biomarkers discriminating UIAs patients and control participants in training set, (C) ROC curve of potential plasma metabolites biomarkers discriminating UIAs patients and control participants in validation set, (D) Scatter plot showing model prediction performance in discriminating

UIA patients and control participants. Based on the training set and verification set data, the logistic regression was used to build the optimal biomarkers model. The horizontal coordinate is the actual group of the sample, and the vertical coordinates are the possibility of the sample's group predicted by the model. The dotted line is the cuff-off value of 0.5. (E) ROC curve of potential plasma metabolites biomarkers discriminating RIA patients and UIA patients in training set. (F) ROC curve of potential plasma metabolites biomarkers discriminating RIA patients and UIA patients in validation set. (G) Scatter plot showing model prediction performance in discriminating RIA patients and UIA patients.

Figure 5

Relative content change of potential biomarkers in training and validation set. (A) Box plots of M6 biomarkers in UIAs patients and control participants. (B) Box plots of M5 biomarkers in RIA patients and UIA patients.

Supplementary Files

This is a list of supplementary files associated with this preprint. Click to download.

- Supplementalfigure1.tif
- Supplementalfigure2.tif
- Supplementalfigure3.tif
- Supplementalfigure4.tif
- GA.png